Research Square

Preprints are preliminary reports that have not undergone peer review.
They should not be considered conclusive, used to inform clinical practice,
or referenced by the media as validated information.

History dependence in synchronization from rate asymmetry and phase weight feedback in adaptive networks

Yousef Jamali

y.jamali@gmail.com

Tarbiat Modares University

Article

Keywords:

Posted Date: November 12th, 2026

DOI: https://doi.org/10.21203/rs.3.rs-11427432/v1

License: This work is licensed under a Creative Commons Attribution 4.0 International License.
Read Full License

Additional Declarations: No competing interests reported.

History dependence in synchronization from rate asymmetry and phase weight feedback in adaptive networks

Yousef Jamali
Complex Systems Laboratory, Department of Applied Mathematics, School of Mathematical Sciences, Tarbiat Modares University, Tehran, Iran
Correspondence: Yousef Jamali (y.jamali@gmail.com)

Abstract

Adaptive networks can exhibit pronounced dependence on dynamical history, but the mechanisms controlling the extent and organization of this dependence are not fully understood. Here we study an adaptive Kuramoto network in which the relative rates of coupling strengthening and weakening are varied while the total adaptation-rate budget is held fixed. Weakening-dominated adaptation produces a substantially broader history-dependent synchronization interval than symmetric adaptation, whereas strengthening-dominated adaptation strongly suppresses it. Cross-initialization of phase and weight histories shows that both components influence the final collective state, while a strong non-additive phase–weight interaction appears in the weakening-dominated regime. This indicates that the observed history dependence is associated with the joint organization of phases and adaptive weights rather than with either subsystem alone. Long-time simulations further show that the resulting low- and high-history regimes remain macroscopically separated over timescales much longer than the microscopic adaptation timescales. A reduced mean-field theory links coherence to the fraction of strengthening edges, yields an adaptive branch relation and fold condition, and identifies an asymmetry-dependent feedback coefficient $\Gamma(\rho)$. The resulting Γ^2 scaling reproduces the observed trend in hysteresis suppression without fitting the numerical widths. Together, these results show how rate asymmetry can regulate both the extent and organization of history-dependent synchronization in adaptive networks.

Introduction

Synchronization is a canonical example of collective behavior in nonlinear systems. Populations of heterogeneous oscillators can spontaneously develop coherent macroscopic motion despite differences in their intrinsic frequencies, and the Kuramoto model has become a standard framework for understanding this transition [1-6]. On complex networks, synchronization depends not only on oscillator heterogeneity and coupling strength but also on connectivity, network heterogeneity, and correlations between structural and dynamical variables [4,5,7].

Many natural and engineered systems, however, violate the assumption that interactions are fixed. In adaptive networks, the states of the interacting units alter the interaction strengths or topology, while the changing interactions feed back onto the node dynamics [8-10]. This reciprocal dependence can generate phenomena that are absent in static networks, including enhanced synchronization, multistability, cluster formation, desynchronization transitions, and path-dependent collective states [11-18]. Phase-oscillator networks provide a particularly transparent setting in which to isolate these mechanisms. Early work showed that phase-dependent plasticity can organize synchronized clusters and store information in coupling patterns [15-17], while more recent studies have demonstrated rich bifurcation structures, recurrent synchronization, dense multistability, and multiple synchronized patterns under adaptive coupling [19-25].

A key ingredient of many adaptive processes is rate asymmetry. Formation and dissolution, potentiation and depression, or reinforcement and decay need not occur at the same rate. Asymmetric adaptation has been shown to reorganize the dynamics of oscillator networks and can generate recurrent synchronization or complex bifurcation structures [20,21]. Adaptive feedback can also enhance synchronization or drive abrupt and explosive transitions with hysteresis [26-32]. These results suggest that asymmetry is not merely a quantitative perturbation to a learning rule but can change the macroscopic organization of an adaptive system.

Two mechanistic questions remain important. First, how does the *relative* rate of strengthening and weakening control history dependence when the overall adaptation-

rate scale is controlled? Varying one rate while fixing the other changes both the asymmetry and the characteristic adaptation speed, making their effects difficult to separate. Second, when the same external parameters support different history-conditioned collective states, where is the retained history encoded? It may reside predominantly in oscillator phases, in the adaptive weights, or in correlations between the two. The distinction is important because identical mean coupling strength can have different dynamical consequences depending on which oscillator pairs carry the strongest interactions.

Here we address these questions using a sparse adaptive Kuramoto network with a fixed binary topology and phase-dependent coupling weights. Existing edges strengthen at rate α when the phase similarity of their endpoints exceeds a threshold and weaken at rate β otherwise. The asymmetry parameter is $\rho = \alpha/\beta$. We first map the synchronization landscape and establish a pronounced forward-backward hysteresis. We then isolate the effect of rate asymmetry by holding $\alpha + \beta$ fixed while comparing weakening-dominated, symmetric, and strengthening-dominated adaptation. Weakening-dominated dynamics strongly broaden the history-dependent regime, whereas strengthening-dominated adaptation nearly removes it. Cross-initialization of phase and weight states shows that the most persistent history dependence is non-additive and belongs to the coupled phase-weight configuration. Finally, a reduced theory connects the coherence-dependent weight response to the Kuramoto self-consistency condition, derives the fold criterion for a hysteretic branch, and explains why the corresponding feedback weakens as ρ increases. The model and coherence-coupling feedback are summarized schematically in Fig. 1. The combined numerical and analytical results identify a simple route by which local asymmetric adaptation controls macroscopic memory-like behavior in adaptive dynamical networks.

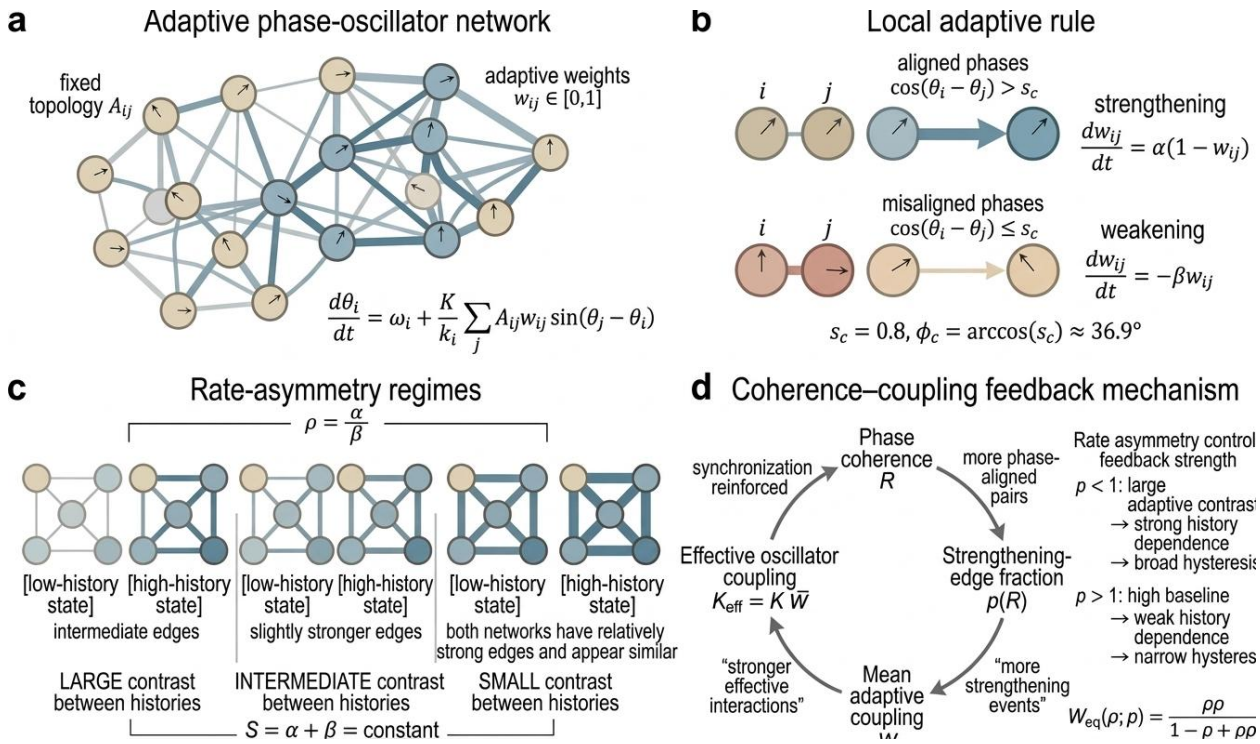


Figure 1 | Adaptive phase-oscillator model and coherence-coupling feedback. a, Oscillators are connected by a fixed sparse network whose existing edge weights w_{ij} evolve dynamically. **b**, Edges strengthen at rate α when $\cos(\theta_i - \theta_j) > s_c$ and weaken at rate β otherwise. **c**, The ratio $\rho = \alpha/\beta$ distinguishes weakening-dominated, symmetric, and strengthening-dominated adaptation. **d**, Schematic positive feedback in which phase coherence increases the strengthening-edge fraction, raises effective coupling, and promotes further coherence.

Results

Adaptive coupling creates a broad history-dependent synchronization regime

We first characterized the collective dynamics over global coupling strength K and adaptation-rate ratio $\rho = \alpha/\beta$. In this exploratory scan, $\beta = 0.1$ was fixed while $\alpha = \rho\beta$, so both the rate ratio and the overall adaptation-rate scale varied. The resulting phase diagram showed a systematic shift of the synchronization transition toward lower K as strengthening became faster (Fig. 2a-c). The approximate $R = 0.5$ crossing decreased from $K_c \simeq 2.29$ at $\rho = 0.01$ to 1.77 at $\rho = 0.1$, 0.93 at $\rho = 1$, and about 0.79 at $\rho = 10$

and 100. Across the scan, the mean coupling weight and synchronization level were strongly correlated ($r \approx 0.90$), consistent with positive feedback between coherence and adaptive coupling. The corresponding weight landscape, weight variability, R-W association, and comparison of three transition estimators are shown in Supplementary Fig. S1.

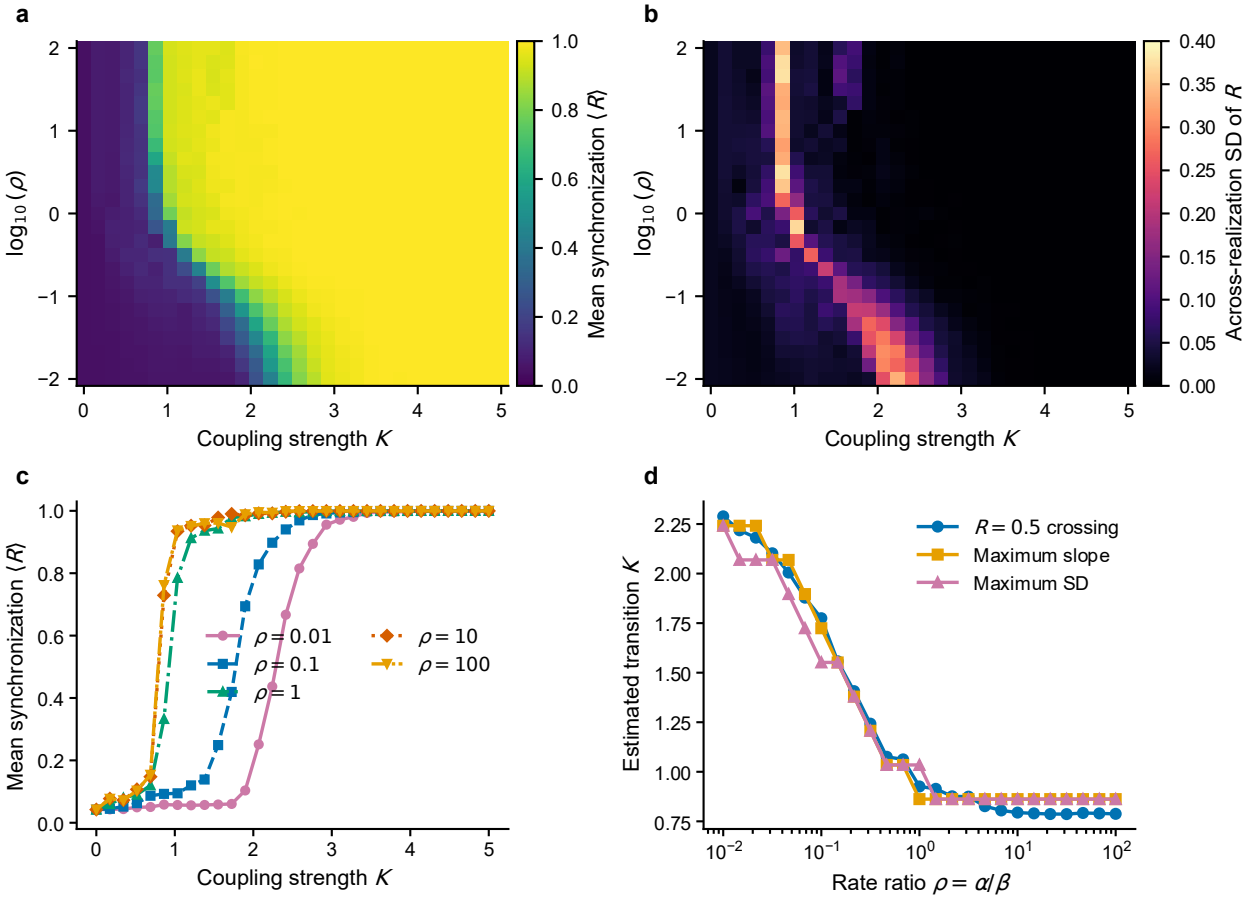


Figure 2 | Global synchronization landscape under adaptive coupling. a, Mean Kuramoto order parameter $\langle R \rangle$ across coupling strength K and adaptation-rate ratio ρ in the exploratory scan with fixed $\beta = 0.1$. **b**, Across-realization standard deviation of R. **c**, Representative synchronization curves at selected ρ; marker and line-style differences provide redundant encoding in addition to color. **d**, Three complementary transition estimators: the $R = 0.5$ crossing, maximum local slope, and maximum across-realization SD. The exploratory scan characterizes phenomenology; controlled rate-asymmetry tests at fixed rate budget are shown in Fig. 4.

To test whether this feedback produces path dependence, we performed continuation in K for weakening-dominated adaptation ($\alpha = 0.01$, $\beta = 0.1$, $\rho = 0.1$). The forward branch remained weakly synchronized to substantially larger K than the backward branch, which retained near-complete synchronization as K was reduced (Fig. 3a). The mean $R = 0.5$ crossing occurred at $K_{\uparrow} \simeq 1.381$ in the forward sweep and at $K_{\downarrow} \simeq 0.463$ in the backward sweep, giving a hysteresis width

$$\Delta K = K_{\uparrow} - K_{\downarrow} \simeq 0.917.$$

The largest mean branch separation was approximately 0.890 near $K \simeq 0.64$, and the absolute loop area was approximately 1.058. Thus identical external coupling can support macroscopically distinct synchronization levels depending on the path by which the adaptive state is prepared. Realization-level continuation curves and the distributions of crossing locations, loop widths, loop areas, and maximum branch gaps are reported in Supplementary Fig. S2.

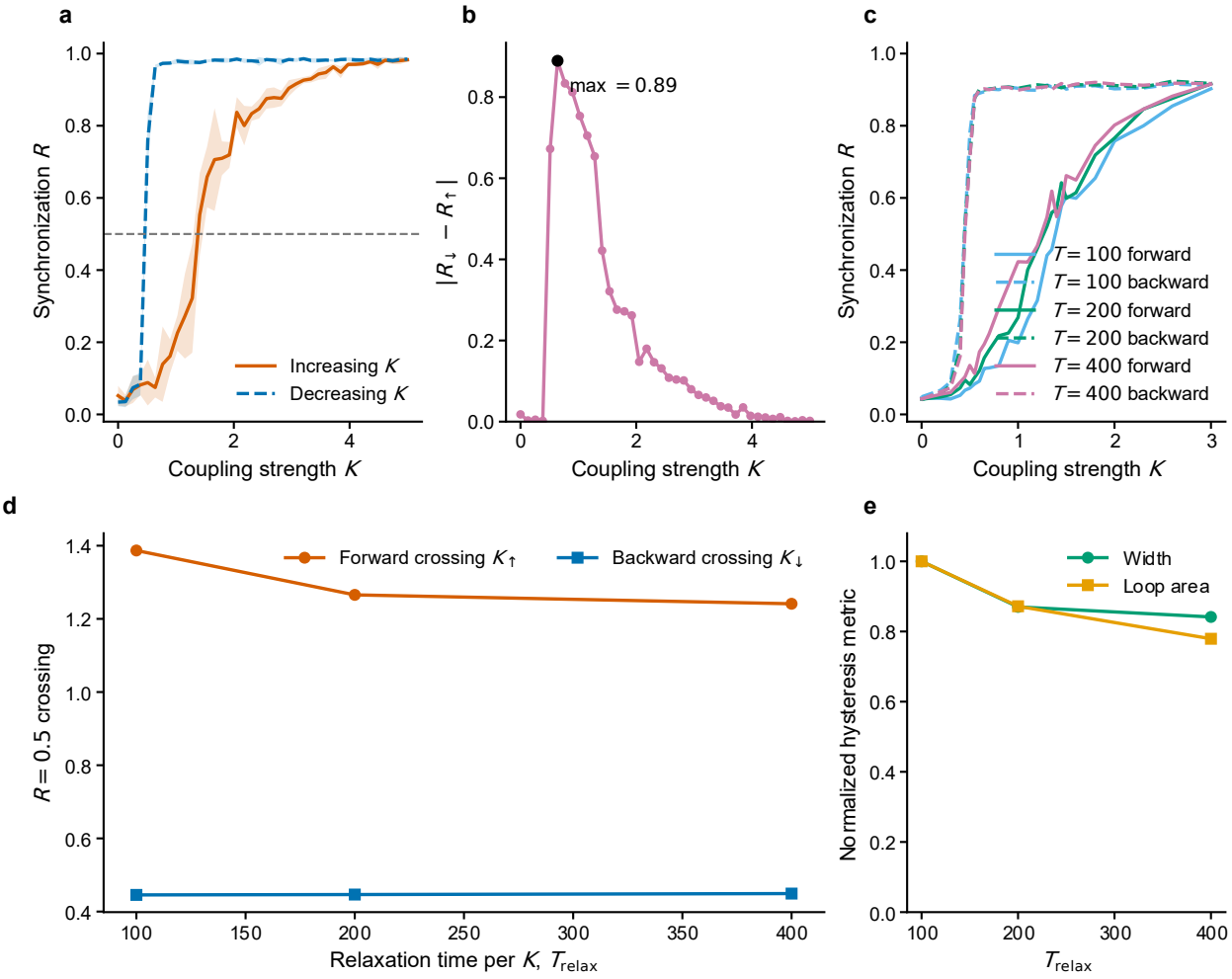


Figure 3 | Hysteretic synchronization and relaxation-time robustness. a, Forward and backward continuation in K at $\rho = 0.1$; shaded regions show across-realization SD. **b**, Absolute branch separation $|R_{\downarrow} - R_{\uparrow}|$. **c**, Forward and backward branches for $T_{\mathrm{relax}} = 100$, 200, and 400. **d**, Forward and backward $R = 0.5$ crossings versus relaxation time. **e**, Hysteresis width and absolute loop area, each normalized to its value at $T_{\mathrm{relax}} = 100$. Persistence of a large residual loop with increasing relaxation time argues against a purely short-sweep artifact.

Finite dwell times can generate dynamic hysteresis even in systems with a unique asymptotic state. We therefore repeated the continuation while increasing the relaxation time per coupling value from $T_{\mathrm{relax}} = 100$ to 200 and 400 (Fig. 3b-e). The hysteresis width decreased from approximately 0.941 to 0.819 and 0.792, respectively, while the backward crossing remained close to $K \simeq 0.45$. The loop area likewise decreased from 0.903 to 0.787 and 0.703, but remained substantial at the longest relaxation time. The

shift of the forward threshold shows that part of the loop is rate dependent, yet the large residual separation indicates robust history dependence that is not explained by a short sweep transient alone.

Controlled rate asymmetry reorganizes the hysteretic interval

The exploratory scan does not isolate asymmetry because changing α at fixed β also changes the total adaptation-rate scale. We therefore imposed a fixed rate budget

$$S = \alpha + \beta = 0.2,$$

and parameterized the two rates as

$$\alpha = \frac{S\rho}{1+\rho}, \qquad \beta = \frac{S}{1+\rho}.$$

This protocol keeps the total strengthening-plus-weakening rate fixed while changing their directional balance. We compared $\rho = 0.1$, 1, and 10 using matched network, frequency, and initial-phase realizations.

The effect on history dependence was pronounced (Fig. 4a-d). For weakening-dominated adaptation ($\rho = 0.1$), the low-history and high-history branches crossed $R = 0.5$ at $K_L \simeq 1.248$ and $K_H \simeq 0.497$, respectively. The corresponding width was

$$\Delta K_{0.1} = 0.750 \quad [0.721, 0.772],$$

where brackets denote a bootstrap 95% confidence interval. Symmetric adaptation retained a substantial history-dependent region but with a smaller width,

$$\Delta K_1 = 0.388 \quad [0.373, 0.406].$$

For strengthening-dominated adaptation, the two crossings nearly coincided,

$$\Delta K_{10} = 0.021 \quad [0.011, 0.030].$$

Relative to the symmetric case, weakening-dominated adaptation broadened the interval by a factor of about 1.93, whereas strengthening-dominated adaptation reduced it to about 5.5% of the symmetric width. The controlled experiment therefore shows that rate asymmetry regulates the *extent* of macroscopic history dependence, rather than

merely shifting a synchronization threshold. Symmetric adaptation still supports hysteresis; asymmetry determines how strongly that history dependence is expressed.

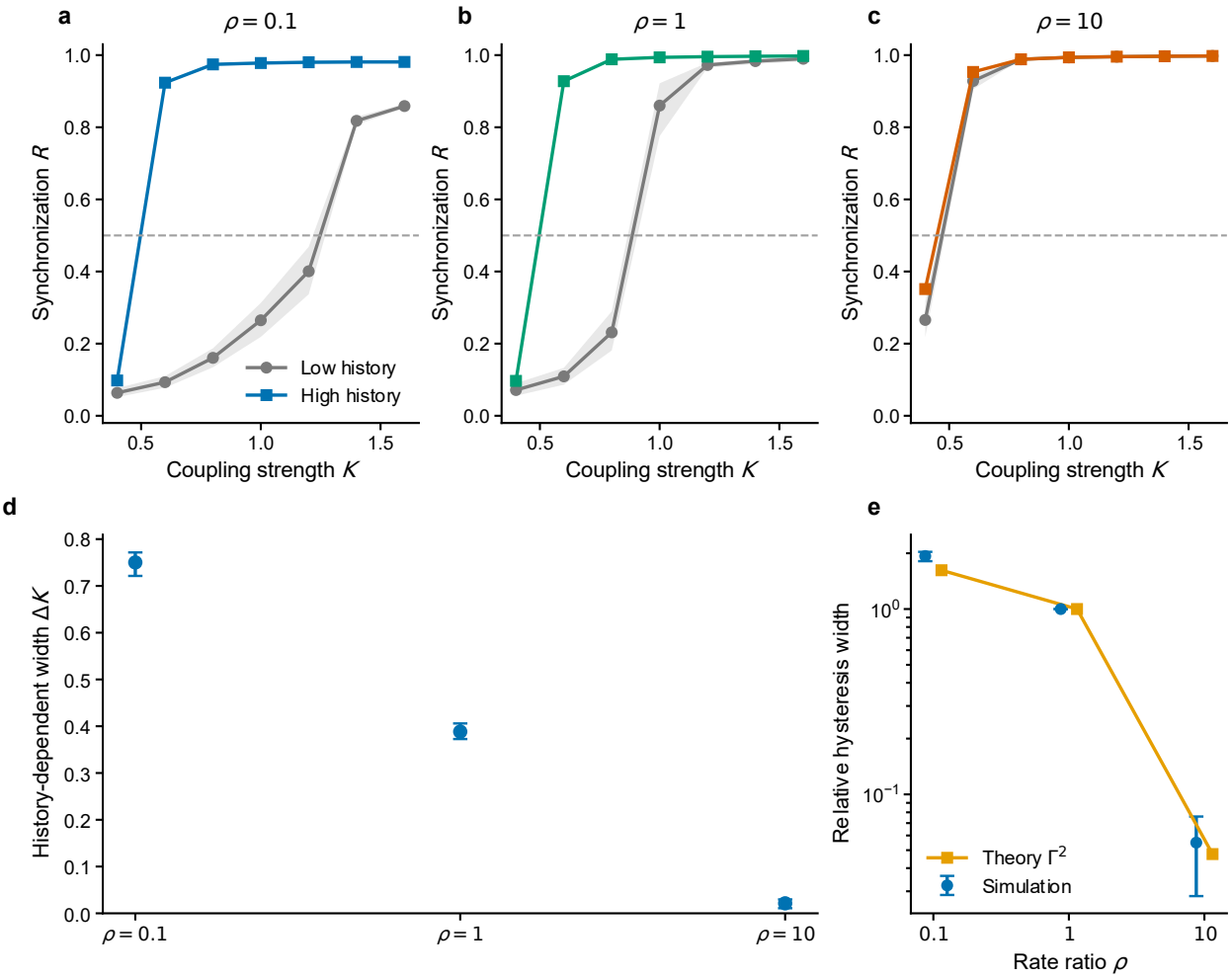


Figure 4 | Adaptation-rate asymmetry controls the history-dependent regime. a-c, Low- and high-history branches under a fixed rate budget $\alpha + \beta = 0.2$ for $\rho = 0.1$, 1, and 10. Shading denotes bootstrap 95% confidence intervals across matched realizations. **d**, History-dependent width ΔK obtained from the low- and high-history $R = 0.5$ crossings, with matched-bootstrap 95% confidence intervals. **e**, Relative numerical widths compared with the reduced-theory scaling $\Gamma(\rho)^2$; the vertical axis is logarithmic.

Cross-initialization reveals non-additive phase-weight memory

We next asked which component of the adaptive state carries the history. For each realization, continuation generated a low-history state $(\boldsymbol{\theta}_L, \mathbf{W}_L)$ and a high-history state $(\boldsymbol{\theta}_H, \mathbf{W}_H)$. We then recombined phases and weights to create four initial conditions: $LL = (\boldsymbol{\theta}_L, \mathbf{W}_L)$, $LH = (\boldsymbol{\theta}_L, \mathbf{W}_H)$, $HL = (\boldsymbol{\theta}_H, \mathbf{W}_L)$, and $HH = (\boldsymbol{\theta}_H, \mathbf{W}_H)$. Their final synchronization levels at $K = 0.8$ are shown for $\rho = 0.1$, 1, and 10 in Fig. 5a-c, with the non-additive interaction and factorial phase/weight effects summarized in Fig. 5d,e.

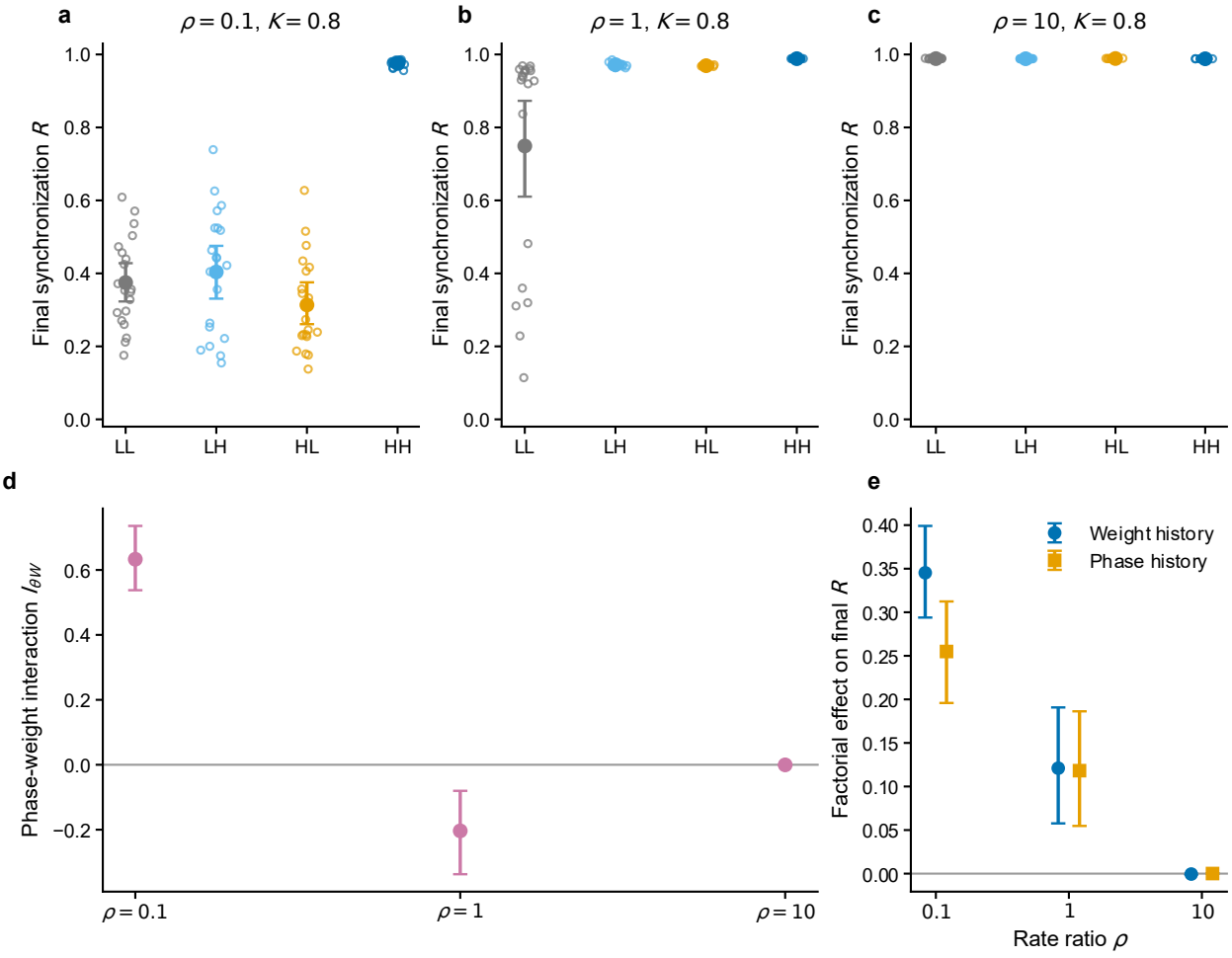


Figure 5 | Cross-initialization reveals non-additive phase-weight memory. a-c, Final synchronization across LL, LH, HL, and HH initializations at $K = 0.8$ for $\rho = 0.1$, 1, and 10. Open symbols show individual realizations and filled symbols show bootstrap means with 95% confidence intervals. **d**, Non-additive phase-weight interaction $I_{\theta W} = R_{HH} - R_{HL} - R_{LH} + R_{LL}$. **e,** Factorial weight-history and phase-history effects, defined as the marginal effect of replacing

the corresponding low-history component by its high-history counterpart while averaging over the state of the other component. Error bars denote bootstrap 95% confidence intervals.

In the strongly history-dependent regime ($\rho = 0.1$, $K = 0.8$), the four conditions evolved to markedly different outcomes:

$$R_{LL} \simeq 0.375, \quad R_{LH} \simeq 0.404, \quad R_{HL} \simeq 0.314, \quad R_{HH} \simeq 0.975.$$

High-history weights alone therefore did not reproduce the high-history synchronized state, and neither did high-history phases alone.

To separate the average contributions of the two history components, we calculated the factorial weight-history and phase-history effects defined in Methods (Fig. 5e). At $\rho = 0.1$ and $K = 0.8$, both were substantial, with $M_W \simeq 0.345$ and $M_\theta \simeq 0.255$. Thus both the adapted weight configuration and the phase configuration influence the final synchronization level, with a somewhat larger marginal effect of weight history under these conditions. These effects are marginal rather than independent contributions, however, because the same regime exhibits a strong non-additive phase-weight interaction.

The non-additivity of these contributions was quantified by $I_{\theta W}$, defined in Methods, (Fig. 5d). At $\rho = 0.1$ and $K = 0.8$, the interaction was strongly positive,

$$I_{\theta W} \simeq 0.633 \quad [0.538, 0.736],$$

where brackets denote a bootstrap 95% confidence interval. A similarly strong interaction was observed near $K = 0.6$. Therefore, although both phase and weight histories have substantial marginal effects, their combined influence cannot be represented as the sum of two independent contributions. The strongly synchronized high-history state depends on their compatible joint organization.

The organization changed with rate asymmetry. At $\rho = 1$ and $K = 0.8$, $R_{LL} \simeq 0.749$, whereas $R_{LH} \simeq 0.972$, $R_{HL} \simeq 0.969$, and $R_{HH} \simeq 0.988$. Consistently, the factorial effects became smaller and nearly equal, $M_W \simeq 0.121$ and $M_\theta \simeq 0.118$ (Fig. 5e), indicating that

neither history component clearly dominates in the symmetric regime. The interaction became negative ($I_{\theta W} \simeq -0.204$), consistent with saturation near $R = 1$: once either high-history component moves the system close to strong synchronization, little dynamic range remains for the second component to add independently. At $\rho = 10$, all four conditions converged to approximately the same strongly synchronized state ($R \simeq 0.988$), and both factorial effects approached zero (Fig. 5e), consistent with the near-complete loss of sensitivity to preparation history.

This behavior motivates a relational interpretation of memory. A high mean weight is not sufficient if strong edges are no longer associated with phase relationships compatible with the synchronized state. A natural macroscopic quantity is therefore the phase-weight alignment

$$Q = \left\langle w_{ij} \cos\left(\theta_i - \theta_j\right) \right\rangle_E,$$

or, equivalently, the covariance between edge weight and phase similarity. The cross-initialization experiment directly perturbs this correspondence while retaining one subsystem from the high-history state, explaining why HH can remain distinct from both LH and HL. Consistent with this interpretation, random phase initialization alone does not generate a clean high/low bimodality (Supplementary Fig. S3), interpolation to the full high-history weight pattern fails to recover the high state after phase randomization (Supplementary Fig. S4), conditioned states show substantial perturbation robustness (Supplementary Fig. S5), and the earlier $\rho = 0.1$ cross-initialization scan confirms the same phase-weight mechanism across several K values (Supplementary Fig. S6).

History-conditioned states remain separated over long times

To determine whether the observed branch separation survives far beyond the conditioning time, we held low- and high-history states at fixed K for $T = 3200$ in the original weakening-dominated regime ($\alpha = 0.01$, $\beta = 0.1$). At $K = 0.8$, the late-time low-history synchronization was

$$R_{LL} = 0.371 \quad [0.359, 0.383],$$

whereas the high-history state remained near complete synchronization,

$$R_{HH} = 0.989 \quad [0.987,\ 0.991].$$

The paired branch separation was therefore

$$R_{HH} - R_{LL} = 0.618 \quad [0.607,\ 0.629].$$

At $K = 1.0$, the corresponding values were $R_{LL} = 0.446$ and $R_{HH} = 0.992$, giving a separation of 0.546 with a 95% bootstrap interval of $[0.514,0.581]$ (Fig. 6).

The high-history branch was effectively stationary over the late-time window, with mean slopes of order 10^{-8}. The low-history branch retained a much smaller but detectable positive drift, of order 10^{-5}. We therefore describe these states conservatively as persistent history-conditioned regimes rather than claiming a formal proof of two asymptotically stable attractors. Importantly, the hold time is much larger than the microscopic timescales $1/\beta = 10$ and $1/\alpha = 100$, so the observed separation cannot be attributed simply to adaptation not having had time to respond. Per-realization late-time slopes, blockwise changes, tail R-W relations, and paired $HH - LL$ gaps are shown in Supplementary Fig. S7.

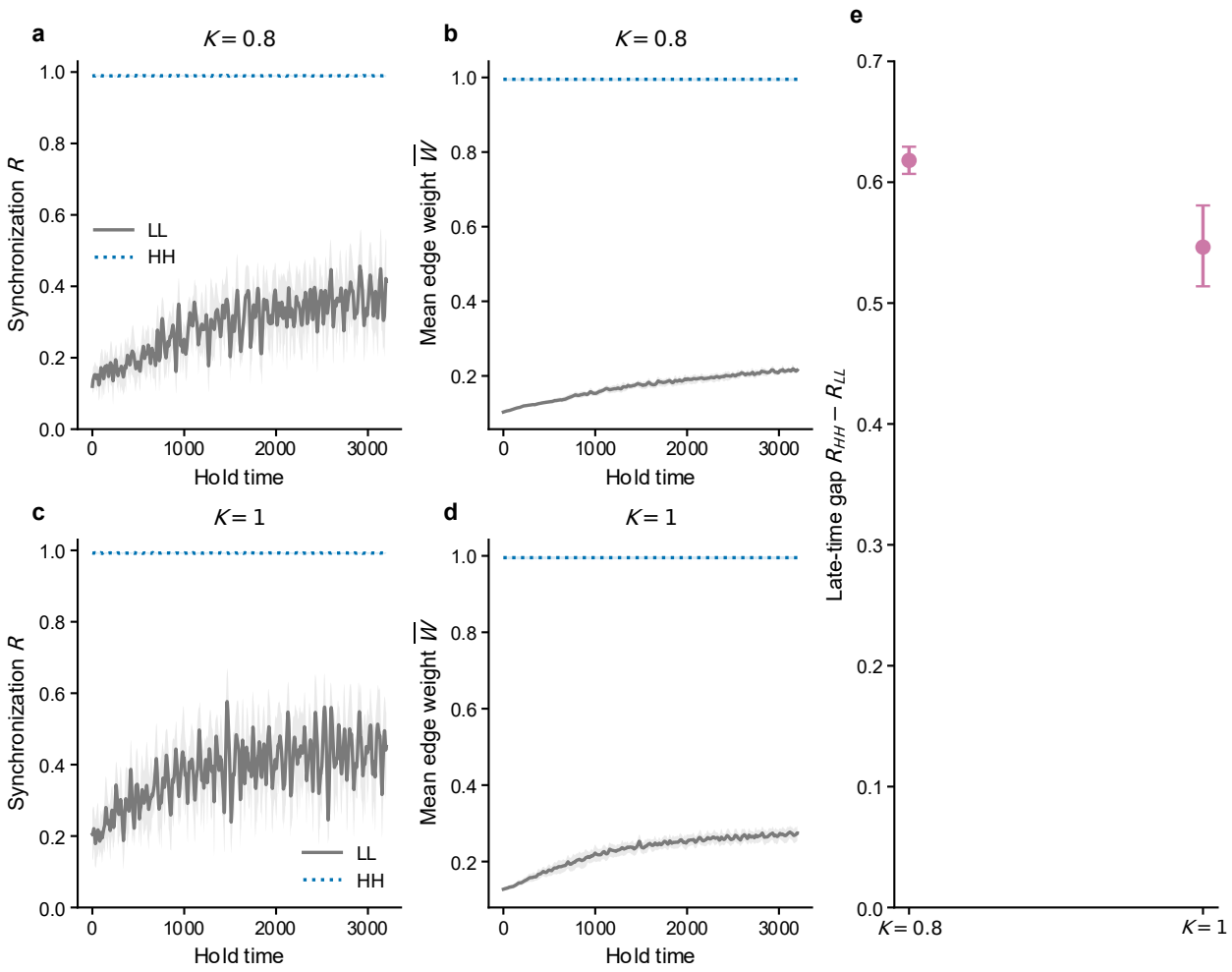


Figure 6 | Long-time persistence of history-conditioned synchronization. a,b, Bootstrap mean trajectories and 95% confidence bands for synchronization R and mean edge weight W at $K = 0.8$. **c,d**, Corresponding trajectories at $K = 1.0$. **e**, Late-time paired branch separation $R_{HH} - R_{LL}$ with bootstrap 95% confidence intervals. The high-history branch is stationary to numerical resolution, whereas the low-history branch shows slow residual relaxation while remaining strongly separated.

Mean-field theory of asymmetry-controlled hysteresis

The numerical results suggest a positive feedback loop: phase coherence increases the fraction of edges that strengthen, larger weights increase the effective coupling, and stronger coupling promotes further coherence. We developed a reduced mean-field

description that makes this loop explicit and quantifies how its strength depends on the rate ratio ρ.

Let

$$C_{ij} = H\left[\cos\left(\theta_i - \theta_j\right) - s_c\right]$$

indicate whether an edge is instantaneously in the strengthening state, and let $p = \langle C_{ij} \rangle_E$ be the fraction of strengthening edges. Neglecting phase-weight correlations at first, the mean edge weight $W = \langle w_{ij} \rangle_E$ obeys

$$\dot{W} = \alpha p(1 - W) - \beta(1 - p)W.$$

For fixed p, the stationary response is

$$W_{\mathrm{eq}}(p; \rho) = \frac{\rho p}{1 - p + \rho p}.$$

In the incoherent limit, phase differences are uniformly distributed and the strengthening probability is

$$p_0 = \frac{\phi_c}{\pi}, \qquad \phi_c = \arccos s_c.$$

With $s_c = 0.8$, $p_0 \simeq 0.2048$. The corresponding incoherent baseline weight is

$$W_0(\rho) = \frac{\rho p_0}{1 + (\rho - 1)p_0}.$$

The factorized theory therefore predicts $W_0 \simeq 0.025$ for $\rho = 0.1$, 0.205 for $\rho = 1$, and 0.720 for $\rho = 10$. A useful measure of the available low-to-high coupling range is the *adaptive contrast*

$$D(\rho) = 1 - W_0(\rho) = \frac{1 - p_0}{1 + (\rho - 1)p_0}.$$

Thus $D \simeq 0.975$, 0.795, and 0.280 for $\rho = 0.1$, 1, and 10, respectively. Weakening-dominated adaptation can therefore separate a weakly coupled incoherent history from a strongly coupled coherent history over a much larger dynamical range, whereas strengthening-dominated adaptation maintains substantial coupling even when phases are disordered.

To connect this adaptive response to synchronization, we use the degree-normalized annealed approximation appropriate to the relatively homogeneous Erdős-Rényi network and write the effective oscillator coupling as

$$J = KW_{\mathrm{eq}}(R;\rho).$$

For a symmetric unimodal natural-frequency density $g(\omega)$ in the rotating frame, the stationary Kuramoto self-consistency condition can be written as [2,3,33-37]

$$1 = J\int_{-\pi/2}^{\pi/2}\cos^2 u\ g(JR\sin u)\,du.$$

This relation defines the effective coupling required to sustain a given coherence, $J = \mathcal{J}(R)$. The stationary adaptive branch must satisfy both the oscillator and weight conditions, giving the central branch equation

$$\boxed{K(R;\rho) = \frac{\mathcal{J}(R)}{W_{\mathrm{eq}}(R;\rho)}}.$$

This branch equation has a direct mechanistic interpretation: the numerator is the coupling demanded by the oscillator population to maintain coherence R, whereas the denominator is the coherence-dependent amplification supplied by adaptation. A fold of the adaptive synchronization branch occurs when

$$\frac{dK}{dR} = 0,$$

or equivalently

$$\boxed{\frac{d\ln\mathcal{J}}{dR} = \frac{d\ln W_{\mathrm{eq}}}{dR}}.$$

Backward bending therefore appears when the adaptive increase of coupling with coherence is sufficiently strong relative to the intrinsic coupling requirement of the oscillator population.

Near incoherence, the probability that a random edge lies inside the strengthening window has the expansion

$$p(R) = p_0 + p_2 R^2 + O(R^4), \qquad p_2 = \frac{2\sin\phi_c}{\pi}.$$

The corresponding adaptive response is

$$W_{\mathrm{eq}}(R) = W_0 + W_2 R^2 + O(R^4),$$

with

$$W_2 = \frac{\rho p_2}{[1 + (\rho - 1)p_0]^2},$$

and hence

$$\frac{W_2}{W_0} = \frac{p_2}{p_0[1 + (\rho - 1)p_0]}.$$

The Kuramoto self-consistency relation likewise gives

$$\mathcal{J}(R) = J_c\left[1 + c_g R^2 + O(R^4)\right], \qquad J_c = \frac{2}{\pi g(0)},$$

where

$$c_g = -\frac{g''(0)}{2\pi^2 g(0)^3}.$$

For the Gaussian frequency distribution used here, $c_g = 1/\pi$. Combining the oscillator and adaptive expansions yields

$$K(R) = K_0[1 - \Gamma(\rho)R^2 + O(R^4)], \qquad K_0 = \frac{J_c}{W_0},$$

with the asymmetry-dependent feedback coefficient

$$\boxed{\Gamma(\rho) = \frac{p_2}{p_0[1 + (\rho - 1)p_0]} - \frac{1}{\pi}}.$$

The coefficient decreases strongly across the controlled asymmetries: $\Gamma(0.1) \simeq 1.97$, $\Gamma(1) \simeq 1.55$, and $\Gamma(10) \simeq 0.34$. Positive Γ means that the adaptive response initially grows faster than the intrinsic coupling requirement, so the synchronized branch bends toward lower external coupling as R increases. This local backward bending is the ingredient required for a subcritical hysteretic onset. The full parameter dependence of

$W_0(\rho)$, the adaptive contrast $1 - W_0$, $\Gamma(\rho)$, and the leading Γ^2 scaling is shown in Supplementary Fig. S8.

The same result can be expressed using the generic quintic amplitude equation

$$\tau_R \dot{R} = \mu R + aR^3 - bR^5 + \cdots, \qquad b > 0,$$

with $a \propto \Gamma(\rho)$. The finite-amplitude branch then undergoes a saddle-node at

$$\mu_{\mathrm{SN}} = -\frac{a^2}{4b},$$

so, provided the higher-order saturation varies more weakly with ρ, the leading hysteretic scale obeys

$$\Delta K_{\mathrm{hyst}} \propto \Gamma(\rho)^2.$$

Without fitting the simulated widths, this scaling captures the relative suppression well (Fig. 4e). Normalized to $\rho = 1$, the theory predicts width ratios of approximately 1.62 at $\rho = 0.1$ and 0.048 at $\rho = 10$, compared with numerical ratios of 1.93 and 0.055. The factorized closure also predicts that the local backward-bending coefficient ultimately changes sign at $\rho \simeq 24.7$ for the present threshold; because this value lies outside the controlled numerical comparison, we treat it as a qualitative theoretical prediction rather than a measured bifurcation point (Supplementary Note S4).

The reduced theory is not an exact bifurcation solution of the sparse adaptive network. It neglects finite-size fluctuations, higher phase harmonics, degree-weight correlations, and, most importantly, the phase-weight correlations that become strongest inside the history-dependent regime. Its value is that it converts the numerical trend into an explicit competition between the coupling required by the oscillators and the coupling generated by adaptation.

Phase-weight correlations provide a memory variable

The factorized closure also reveals why a scalar mean weight is insufficient to describe the strongest memory regime. Averaging the microscopic adaptation equation *without* assuming independence between edge weight and strengthening state gives the exact identity

$$\boxed{\dot{W} = \alpha p(1 - W) - \beta(1 - p)W + (\beta - \alpha)\mathrm{Cov}(C, w)}.$$

Because aligned edges are preferentially strengthened, the dynamics naturally generates $\mathrm{Cov}(C, w) > 0$. For weakening-dominated adaptation ($\beta > \alpha$), this correlation contributes positively to the mean-weight dynamics. For symmetric adaptation ($\alpha = \beta$), the covariance term cancels exactly from the equation for W, while for strengthening-dominated adaptation its contribution changes sign. Thus rate asymmetry affects not only the scalar weight response but also how correlations between dynamical state and adaptive coupling feed back onto the collective dynamics.

A continuous measure of this relational organization is

$$\boxed{Q = \left\langle w_{ij}\cos\left(\theta_i - \theta_j\right)\right\rangle_E}$$

which can be decomposed as

$$Q = W\langle\cos\Delta\rangle_E + \mathrm{Cov}(w, \cos\Delta).$$

The covariance term distinguishes weight configurations with the same mean W but different placement of strong edges relative to the phase pattern. This provides a direct theoretical interpretation of the cross-initialization results: HH preserves the correspondence between strong edges and compatible phase relationships, whereas LH and HL disrupt one side of that correspondence. The large positive $I_{\theta W}$ at $\rho = 0.1$ is therefore evidence that the relevant memory variable is not R or W separately, but their joint phase-weight organization. A two-class edge closure that resolves coherent and incoherent edge populations makes this correlation mechanism explicit and is developed in Supplementary Note S5.

Discussion

Our results show that adaptation-rate asymmetry controls the extent and organization of history-dependent synchronization in an adaptive oscillator network. The main effect is not the mere existence of hysteresis. Adaptive oscillator systems are already known to support multistability, abrupt transitions, synchronized clusters, and recurrent synchronization [15-32]. Rather, the controlled rate-budget experiment demonstrates

that the *direction* of asymmetry strongly regulates the parameter interval over which dynamical history remains macroscopically visible. Weakening-dominated adaptation nearly doubles the history-dependent interval relative to symmetric adaptation, whereas strengthening-dominated adaptation almost removes it.

The reduced theory explains this behavior through adaptive contrast and, more generally, through the branch relation $K(R;\rho) = \mathcal{J}(R)/W_{\mathrm{eq}}(R;\rho)$, which makes the fold mechanism explicit. Detailed derivations and the higher-order correlation closure are given in Supplementary Notes S1-S5. Even in an incoherent population, about 20% of random phase differences satisfy the strengthening threshold used here. If strengthening is slow relative to weakening, these accidental alignments are insufficient to maintain large weights, and the incoherent baseline coupling remains very small. A coherent history, by contrast, can keep many edges persistently inside the strengthening window and build a strongly coupled state. The adaptive network can therefore separate low- and high-history trajectories over a large region of parameter space. When strengthening dominates, the same accidental alignments rapidly build coupling and decay is slow; the nominally low-history state becomes strongly coupled, compressing the distinction between histories.

This mechanism is consistent with earlier work showing that activity-dependent weights can enhance synchronization and generate multiple collective regimes [11-18], and with recent analyses of adaptive Kuramoto systems in which adaptation produces complex bifurcation structures, continuum multistability, and finite-size switching phenomena [21-23]. It is also conceptually related to adaptive explosive synchronization, where positive feedback between coherence and coupling produces abrupt collective transitions [28-32]. The present contribution is to isolate a simple rate-ratio control of this feedback and connect it quantitatively to the width of the history-dependent regime.

The cross-initialization experiment shows that adaptive history cannot generally be assigned to phases or coupling weights independently. In the weakening-dominated regime, both components have substantial marginal effects, but their strong positive interaction shows that the synchronized history-conditioned state depends primarily on their compatibility. This supports a relational interpretation of memory: what matters is

not only how strong the interactions are, but which oscillator pairs carry those interactions relative to the phase configuration. The covariance term in the reduced weight dynamics and the alignment variable Q provide natural macroscopic representations of this organization.

Rate asymmetry also changes the organization of this memory. Under weakening-dominated adaptation, phase and weight histories act synergistically; under symmetric adaptation, they become more redundant because either high-history component can move the system close to strong synchronization; and under strengthening-dominated adaptation, sensitivity to either component largely disappears. Thus increasing ρ changes not only the width of the hysteretic regime but also how dynamical history is distributed across the adaptive state.

The notion of memory used here is therefore specific. We do not claim associative recall or explicit information storage. Memory denotes persistent path dependence: the current macroscopic state depends on how the adaptive system reached the present parameter values. In this operational sense, the network retains a dynamical history in the joint state $(\boldsymbol{\theta}, \mathbf{W})$. Such relational memory may be relevant more broadly in adaptive systems where slow interactions and fast states coevolve. In neural settings, potentiation and depression are well known to be temporally asymmetric [38-42], and recent modeling work shows that asymmetry in synaptic adaptation can reshape attractor structure and pathological synchronization [43]. Related studies of adaptive modularity, heterogeneous adaptation, and cluster synchronization emphasize that correlations between interaction structure and collective state can organize multiple dynamical patterns [44-51]. Slow synaptic variables have also been proposed as a substrate for working memory [52]. The present model is deliberately more abstract, but it isolates a general physical principle: the balance between reinforcement and decay can determine whether adaptive feedback preserves or erases macroscopic history.

The relational interpretation also suggests experimentally testable analogies beyond neural plasticity, although these should be viewed as transfers of mechanism rather than direct applications of the present model. Reduced power-network models and droop-controlled inverter microgrids can be written as nonuniform or generalized

Kuramoto systems [53,54]. In such systems, if controller-mediated effective couplings adapt to local phase or power mismatch, the present results motivate asking whether recovery from a disturbance depends not only on the mean control gain but also on which links carry large gains relative to the phase-angle pattern. The analogy is more direct in memristive and electronic oscillator networks: memristive elements have been used to implement adaptive couplings whose conductance evolves with state mismatch, physical oscillator experiments show phase locking mediated by memristive coupling, and oscillator ensembles can retain a dependence on the initial states of the coupling elements [55-57]. Phase-oscillator coordination has likewise been used in robotic control, from oscillator-based central pattern generators to recent decentralized multi-robot exploration schemes in which locally coupled phases transmit coordination information [58,59]. At a more abstract level, adaptive-network models of social influence couple individual states to evolving social ties and show that this feedback can reorganize consensus and polarization [60,61]. A corresponding social analogy is that two groups with similar aggregate states and similar overall interaction-strength statistics could nevertheless respond differently if strong influence relationships are aligned with different subsets of individual states. Because these social models use different state variables and often adaptive topology rather than continuous edge weights, this comparison is a conceptual analogy rather than a direct application of the present oscillator model.

Across these settings, the clearest general prediction is a distribution-preserving shuffling test. If history is relational, preserving the instantaneous synchronization level, the mean coupling weight, and even the full marginal distribution of edge weights while randomly permuting those weights among edges should alter subsequent dynamics by destroying the correspondence between coupling strength and pairwise phase relation. Conversely, reinstating the matched state-coupling configuration should recover a previous collective regime more effectively than restoring either the dynamical state or the coupling pattern alone. This also yields a measurable prediction: the alignment variable Q, or an equivalent weight-state covariance, should carry more information about subsequent synchronization or recovery than the mean weight alone. Such

perturbation experiments would directly distinguish relational memory from memory encoded only in node states or in the marginal distribution of coupling strengths.

The long-time tests strengthen the interpretation of the continuation results by showing that history-conditioned states remain macroscopically separated far beyond the microscopic adaptation timescales. The high-history branch is effectively stationary over the simulated interval, whereas the low-history branch retains a small residual drift. We therefore interpret the observations as persistent history-conditioned regimes and robust hysteresis, while avoiding the stronger claim that both branches have been proven to be asymptotically stable attractors.

Several limitations define the scope of the results. We use a single sparse Erdős-Rényi topology with $N = 500$ and fixed binary adjacency. The model therefore concerns adaptive coupling weights rather than structural rewiring. Quantitative transition locations can depend on network size, degree heterogeneity, and topology [4,5,23,36,37]. The hard similarity threshold is chosen for mechanistic transparency; smooth learning functions may alter quantitative boundaries while preserving the same positive-feedback logic. In addition, fixing $\alpha + \beta$ controls the overall rate budget but not the exact state-dependent relaxation rate, which remains $\lambda_W = \alpha p + \beta(1 - p)$. Finally, the factorized theory neglects the very phase-weight correlations that become important in the strongest-memory regime. A natural next step is a closed low-dimensional description in terms of (R, W, Q) or an equivalent covariance variable.

Despite these limitations, the numerical and theoretical results support a unified mechanism. Phase coherence changes which interactions strengthen; the resulting weights alter effective coupling; and rate asymmetry determines how strongly this feedback distinguishes different histories. Weakening-dominated adaptation creates a large low-to-high coupling contrast and a broad hysteretic regime, while strengthening-dominated adaptation raises the low-coherence coupling floor and collapses the distinction between histories. Cross-initialization shows that, where history dependence is strongest, it is stored in the joint phase-weight configuration rather than in either subsystem alone.

Conclusions

In this study, we examined how strengthening–weakening rate asymmetry shapes history-dependent synchronization in an adaptive oscillator network. By varying the rate ratio while keeping the total adaptation-rate budget fixed, we found that weakening-dominated adaptation supports a broad history-dependent regime, whereas strengthening-dominated adaptation strongly reduces it. Cross-initialization experiments further showed that the resulting dependence on history cannot be attributed to the phase configuration or adaptive weights independently; instead, it is associated with their joint organization and with non-additive phase–weight interactions.

The reduced theory provides a complementary mechanistic picture. Coherence changes the fraction of strengthening edges, which modifies the mean adaptive coupling and feeds back onto synchronization. This feedback weakens as the strengthening-to-weakening rate ratio increases, and the resulting asymmetry-dependent coefficient $\Gamma(\rho)$ captures the observed trend in hysteresis suppression. Long-time simulations indicate that the low- and high-history regimes can remain well separated over timescales far exceeding the microscopic adaptation timescales, while the residual drift of the low-history branch motivates a cautious interpretation in terms of persistent history-conditioned regimes rather than proven asymptotically stable attractors.

Taken together, the results suggest that rate asymmetry controls not only the extent of history dependence but also how that history is organized across the coupled phase-weight state. More generally, the study illustrates how local adaptive rules can regulate macroscopic path dependence through correlations between dynamical states and interaction strengths. Extending this framework to heterogeneous adaptation, evolving topology, and reduced descriptions that explicitly track phase-weight correlations may help clarify how similar mechanisms operate in broader classes of adaptive dynamical networks. These results therefore motivate a broader, testable hypothesis: in adaptive networks, macroscopic memory may reside not in the dynamical states or interaction strengths separately, but in the correlations that bind them.

Methods

Adaptive oscillator network

We consider $N = 500$ phase oscillators on an undirected Erdős-Rényi network with edge probability $p_{\mathrm{edge}} = 0.05$. The binary adjacency matrix A_{ij} is symmetric and fixed throughout each simulation. Oscillator phases evolve according to

$$\dot{\theta}_i = \omega_i + \frac{K}{k_i}\sum_j A_{ij}\, w_{ij}\sin\big(\theta_j - \theta_i\big),$$

where $k_i = \sum_j A_{ij}$ is the degree, K is the global coupling strength, and $w_{ij} = w_{ji} \in [0,1]$ is the adaptive weight of an existing edge. Degree normalization reduces trivial variation of local input with node degree. Natural frequencies are independently drawn from a Gaussian distribution with mean $\omega_0 = 1$ and standard deviation $\sigma_\omega = 0.1$. The common frequency offset is immaterial to phase differences; theoretical calculations are performed in the corresponding rotating frame.

The initial weight on every existing edge is $w_{ij}(0) = 0.5$. Unless a continuation protocol supplies the initial condition, phases are sampled independently with $0 \le \theta_i(0) < 2\pi$.

Phase-dependent weight adaptation

Define edge similarity

$$s_{ij} = \cos\big(\theta_i - \theta_j\big).$$

The weight dynamics are

$$\dot{w}_{ij} = \begin{cases} \alpha\big(1 - w_{ij}\big), & s_{ij} > s_c, \\ -\beta w_{ij}, & s_{ij} \le s_c, \end{cases}$$

with $s_c = 0.8$. Strengthening therefore occurs for wrapped phase separations smaller than $\phi_c = \arccos(0.8) \simeq 0.6435$ rad. The asymmetry ratio is $\rho = \alpha/\beta$. Because A_{ij} remains fixed, the model represents adaptive coupling weights and not structural rewiring.

Equations were integrated by an explicit Euler scheme with time step $\Delta t = 0.02$. At each step the phase state was advanced and the adaptation rule was then evaluated using the updated phases. Weights were constrained to $[0,1]$. Observables were sampled every 50 integration steps, corresponding to one time unit.

Synchronization was quantified by the Kuramoto order parameter

$$Re^{i\Psi} = \frac{1}{N}\sum_{j=1}^{N} e^{i\theta_j},$$

and the mean edge weight by

$$W = \frac{1}{E}\sum_{(i,j)\in E} w_{ij}.$$

Exploratory phase diagram and continuation

The exploratory synchronization map used 30 equally spaced values of $K \in [0,5]$ and 25 logarithmically spaced values of $\rho \in [10^{-2}, 10^{2}]$. We fixed $\beta = 0.1$ and set $\alpha = \rho\beta$. Each parameter combination was simulated for $T = 200$ with five realizations. Because this protocol changes both rate asymmetry and total adaptation speed, it was used only to map phenomenology.

Hysteresis was measured by full-state continuation. During the forward sweep, the final $(\boldsymbol{\theta}, \mathbf{W})$ state at one coupling value was used to initialize the next larger K while retaining the same natural-frequency vector. The procedure was reversed for the backward sweep. Transition locations were defined by linear interpolation of the $R = 0.5$ crossings. The hysteresis width was $\Delta K = K_{\uparrow} - K_{\downarrow}$, and the absolute loop area was computed by numerical integration of $|R_{\downarrow}(K) - R_{\uparrow}(K)|$. Relaxation robustness was tested using $T_{\mathrm{relax}} = 100$, 200, and 400 per coupling value with 20 realizations.

Fixed-rate-budget asymmetry control

To separate asymmetry from the gross rate scale, final-control simulations fixed

$$S = \alpha + \beta = 0.2$$

and used

$$\alpha = \frac{S\rho}{1+\rho}, \qquad \beta = \frac{S}{1+\rho}$$

for $\rho = 0.1$, 1, and 10. Twenty matched realizations were used at each ratio. The same network, natural-frequency vector, and realization-specific initial phases were retained for cross-ratio comparison. Low-history states were generated by increasing K from 0 in steps of 0.2; high-history states were generated by decreasing K from 3. Each conditioning step was evolved for $T = 200$. The principal target range was $K = 0.4, 0.6, \ldots, 1.6$.

Cross-initialization and long-time tests

For each target parameter set, low- and high-history continuation produced $(\boldsymbol{\theta}_L, \mathbf{W}_L)$ and $(\boldsymbol{\theta}_H, \mathbf{W}_H)$. Their components were recombined into LL, LH, HL, and HH conditions and evolved at identical K, ρ, topology, and natural frequencies for $T_{\mathrm{hold}} = 800$. The factorial weight and phase effects were

$$M_W = \frac{(R_{LH} - R_{LL}) + (R_{HH} - R_{HL})}{2},$$

$$M_\theta = \frac{(R_{HL} - R_{LL}) + (R_{HH} - R_{LH})}{2},$$

and their non-additive interaction was $I_{\theta W} = R_{HH} - R_{HL} - R_{LH} + R_{LL}$.

Long-time persistence was tested in the original $\rho = 0.1$ parameterization, with $\alpha = 0.01$ and $\beta = 0.1$, at $K = 0.8$ and 1.0. Ten matched realizations of low- and high-history states were held for $T = 3200$. Late-time means were calculated over the final 100 sampled observations. Linear slopes over the final half of each trajectory were used as a diagnostic of residual drift.

Reduced mean-field theory

Let $C_{ij} = H\left[\cos\left(\theta_i - \theta_j\right) - s_c\right]$, $p = \langle C_{ij} \rangle_E$, and $W = \langle w_{ij} \rangle_E$. The exact edge average of the microscopic adaptation law is

$$\dot{W} = \alpha p - \beta W + (\beta - \alpha)\langle Cw \rangle.$$

The factorized closure $\langle Cw \rangle \simeq pW$ gives

$$\dot{W} = \alpha p(1 - W) - \beta(1 - p)W$$

and stationary response

$$W_{\mathrm{eq}}(p; \rho) = \frac{\rho p}{1 - p + \rho p}.$$

For fixed p, the relaxation rate toward this response is

$$\lambda_W = \alpha p + \beta(1 - p).$$

Under the fixed-rate-budget parameterization $S = \alpha + \beta$, this becomes

$$\lambda_W(p, \rho) = \frac{S}{1 + \rho}[\rho p + (1 - p)],$$

which clarifies that fixing S controls the gross rate budget but does not impose an identical state-dependent relaxation time.

For an annealed random-edge approximation, define the circular phase harmonics $Z_n = \langle e^{in\theta} \rangle$. The phase-difference density is

$$P_{\Delta}(\Delta) = \frac{1}{2\pi}\left[1 + 2\sum_{n=1}^{\infty} |Z_n|^2 \cos(n\Delta)\right],$$

so integration over the strengthening window gives

$$p = \frac{\phi_c}{\pi} + \frac{2}{\pi}\sum_{n=1}^{\infty} \frac{|Z_n|^2}{n} \sin(n\phi_c).$$

Near incoherence, $Z_1 = Re^{i\Psi}$ and higher harmonics enter at higher order, giving

$$p(R) = p_0 + p_2 R^2 + O(R^4), \qquad p_0 = \frac{\phi_c}{\pi}, \qquad p_2 = \frac{2\sin\phi_c}{\pi}.$$

For the degree-normalized homogeneous-network closure, the oscillator population experiences effective coupling $J = KW_{\mathrm{eq}}$. The stationary Kuramoto self-consistency condition defines $J = \mathcal{J}(R)$ and therefore the adaptive branch

$$K(R; \rho) = \frac{\mathcal{J}(R)}{W_{\mathrm{eq}}(R; \rho)}.$$

Expanding this branch near incoherence yields the coefficient $\Gamma(\rho)$ reported in the Results. Retaining the non-factorized contribution $\langle Cw \rangle = pW + \mathrm{Cov}(C, w)$ yields the exact covariance correction used to interpret phase-weight memory. Full derivations, a von Mises global closure for $p(R)$, the normal-form calculation, the formal crossover estimate, and a two-class coherent/incoherent edge model are provided in Supplementary Notes S1-S5.

Statistical analyses

Across-realization variability is reported using sample standard deviations where appropriate. For the controlled asymmetry, cross-initialization, and long-time experiments, confidence intervals were obtained by nonparametric bootstrap resampling of realizations with 3000 bootstrap samples; intervals correspond to the 2.5th and 97.5th percentiles. Matched contrasts were computed realization by realization before population averaging.

Data availability

The datasets generated and/or analysed during the current study are available from the corresponding author on reasonable request.

Acknowledgements

The author thanks Dr. Tahereh Jamali for her helpful suggestions on the manuscript and guidance on the analysis. This research received no external funding.

Author contributions

Yousef Jamali conceived and designed the study, developed the methodology and software, performed the simulations, analysed and validated the results, prepared the figures, and wrote and revised the manuscript.

Competing interests

The author declares no competing interests.

References

1. Kuramoto, Y. Self-entrainment of a population of coupled non-linear oscillators. In *International Symposium on Mathematical Problems in Theoretical Physics* (ed. Araki, H.) 420-422 (Springer, 1975).
2. Strogatz, S. H. From Kuramoto to Crawford: exploring the onset of synchronization in populations of coupled oscillators. *Physica D* **143**, 1-20 (2000).
3. Acebrón, J. A., Bonilla, L. L., Pérez Vicente, C. J., Ritort, F. & Spigler, R. The Kuramoto model: a simple paradigm for synchronization phenomena. *Rev. Mod. Phys.* **77**, 137-185 (2005).
4. Arenas, A., Díaz-Guilera, A., Kurths, J., Moreno, Y. & Zhou, C. Synchronization in complex networks. *Phys. Rep.* **469**, 93-153 (2008).
5. Rodrigues, F. A., Peron, T. K. D. M., Ji, P. & Kurths, J. The Kuramoto model in complex networks. *Phys. Rep.* **610**, 1-98 (2016).
6. Pikovsky, A., Rosenblum, M. & Kurths, J. *Synchronization: A Universal Concept in Nonlinear Sciences* (Cambridge University Press, 2001).
7. Boccaletti, S., Latora, V., Moreno, Y., Chavez, M. & Hwang, D.-U. Complex networks: structure and dynamics. *Phys. Rep.* **424**, 175-308 (2006).
8. Gross, T. & Blasius, B. Adaptive coevolutionary networks: a review. *J. R. Soc. Interface* **5**, 259-271 (2008).
9. Gross, T. & Sayama, H. (eds) *Adaptive Networks: Theory, Models and Applications* (Springer, 2009).
10. Berner, R., Gross, T., Kuehn, C., Kurths, J. & Yanchuk, S. Adaptive dynamical networks. *Phys. Rep.* **1031**, 1-59 (2023).
11. Sawicki, J. et al. Perspectives on adaptive dynamical systems. *Chaos* **33**, 071501 (2023).
12. Zhou, C. & Kurths, J. Dynamical weights and enhanced synchronization in adaptive complex networks. *Phys. Rev. Lett.* **96**, 164102 (2006).
13. Sorrentino, F. & Ott, E. Adaptive synchronization of dynamics on evolving complex networks. *Phys. Rev. Lett.* **100**, 114101 (2008).

14. Sorrentino, F., Barlev, G., Cohen, A. B. & Ott, E. The stability of adaptive synchronization of chaotic systems. *Chaos* **20**, 013103 (2010).
15. Seliger, P., Young, S. C. & Tsimring, L. S. Plasticity and learning in a network of coupled phase oscillators. *Phys. Rev. E* **65**, 041906 (2002).
16. Aoki, T. & Aoyagi, T. Co-evolution of phases and connection strengths in a network of phase oscillators. *Phys. Rev. Lett.* **102**, 034101 (2009).
17. Aoki, T. & Aoyagi, T. Self-organized network of phase oscillators coupled by activity-dependent interactions. *Phys. Rev. E* **84**, 066109 (2011).
18. Berner, R., Schöll, E. & Yanchuk, S. Multiclusters in networks of adaptively coupled phase oscillators. *SIAM J. Appl. Dyn. Syst.* **18**, 2227-2266 (2019).
19. Berner, R., Vock, S., Schöll, E. & Yanchuk, S. Desynchronization transitions in adaptive networks. *Phys. Rev. Lett.* **126**, 028301 (2021).
20. Thiele, M., Berner, R., Tass, P. A., Schöll, E. & Yanchuk, S. Asymmetric adaptivity induces recurrent synchronization in complex networks. *Chaos* **33**, 023123 (2023).
21. Jüttner, B. & Martens, E. A. Complex dynamics in adaptive phase oscillator networks. *Chaos* **33**, 053106 (2023).
22. Cestnik, R. & Martens, E. A. Continuum limit of the adaptive Kuramoto model. *Chaos* **35**, 013109 (2025).
23. Fialkowski, J. et al. Heterogeneous nucleation in finite-size adaptive dynamical networks. *Phys. Rev. Lett.* **130**, 067402 (2023).
24. Lodi, M., Panahi, S., Sorrentino, F., Torcini, A. & Storace, M. Patterns of synchronized clusters in adaptive networks. *Commun. Phys.* **7**, 198 (2024).
25. Chauhan, K., Khaledi-Nasab, A., Neiman, A. B. & Tass, P. A. Dynamics of phase oscillator networks with synaptic weight and structural plasticity. *Sci. Rep.* **12**, 15003 (2022).
26. Chakravartula, S., Indic, P., Sundaram, B. & Killingback, T. Emergence of local synchronization in neuronal networks with adaptive couplings. *PLoS ONE* **12**, e0178975 (2017).

27. Feketa, P., Schaum, A. & Meurer, T. Synchronization and multicluster capabilities of oscillatory networks with adaptive coupling. *IEEE Trans. Autom. Control* **66**, 3084-3096 (2021).
28. Wang, X., Zheng, Z. & Xu, C. Explosive synchronization in phase oscillator populations with attractive and repulsive adaptive interactions. *Chaos Solitons Fractals* **170**, 113351 (2023).
29. Xu, C., Yu, H. & Guan, S. Dynamical origin of the explosive synchronization with partial adaptive coupling. *Chaos Solitons Fractals* **172**, 113538 (2023).
30. Gómez-Gardeñes, J., Gómez, S., Arenas, A. & Moreno, Y. Explosive synchronization transitions in scale-free networks. *Phys. Rev. Lett.* **106**, 128701 (2011).
31. Boccaletti, S. et al. Explosive transitions in complex networks' structure and dynamics: percolation and synchronization. *Phys. Rep.* **660**, 1-94 (2016).
32. Pazó, D. Thermodynamic limit of the first-order phase transition in the Kuramoto model. *Phys. Rev. E* **72**, 046211 (2005).
33. Ott, E. & Antonsen, T. M. Low dimensional behavior of large systems of globally coupled oscillators. *Chaos* **18**, 037113 (2008).
34. Ott, E. & Antonsen, T. M. Long time evolution of phase oscillator systems. *Chaos* **19**, 023117 (2009).
35. Crawford, J. D. Amplitude expansions for instabilities in populations of globally-coupled oscillators. *J. Stat. Phys.* **74**, 1047-1084 (1994).
36. Restrepo, J. G., Ott, E. & Hunt, B. R. Onset of synchronization in large networks of coupled oscillators. *Phys. Rev. E* **71**, 036151 (2005).
37. Restrepo, J. G., Ott, E. & Hunt, B. R. Synchronization in large directed networks of coupled phase oscillators. *Chaos* **16**, 015107 (2006).
38. Gerstner, W. & Kistler, W. M. Mathematical formulations of Hebbian learning. *Biol. Cybern.* **87**, 404-415 (2002).
39. Bi, G.-Q. & Poo, M.-M. Synaptic modifications in cultured hippocampal neurons: dependence on spike timing, synaptic strength, and postsynaptic cell type. *J. Neurosci.* **18**, 10464-10472 (1998).

40. Abbott, L. F. & Nelson, S. B. Synaptic plasticity: taming the beast. *Nat. Neurosci.* **3**, 1178-1183 (2000).
41. Caporale, N. & Dan, Y. Spike timing-dependent plasticity: a Hebbian learning rule. *Annu. Rev. Neurosci.* **31**, 25-46 (2008).
42. Markram, H., Lübke, J., Frotscher, M. & Sakmann, B. Regulation of synaptic efficacy by coincidence of postsynaptic APs and EPSPs. *Science* **275**, 213-215 (1997).
43. Bi, H., Wang, B., Deng, H., Tian, C. & Zhang, X. Asymmetric synaptic plasticity provides an attractor-based mechanism for theta-gamma coupling and pathological synchronization. *eNeuro* https://doi.org/10.1523/ENEURO.0111-26.2026 (2026).
44. Yuan, W.-J. & Zhou, C. Interplay between structure and dynamics in adaptive complex networks: emergence and amplification of modularity by adaptive dynamics. *Phys. Rev. E* **84**, 016116 (2011).
45. Berner, R., Yanchuk, S. & Schöll, E. What adaptive neuronal networks teach us about power grids. *Phys. Rev. E* **103**, 042315 (2021).
46. Berner, R. & Yanchuk, S. Synchronization in networks with heterogeneous adaptation rules and applications to distance-dependent synaptic plasticity. *Front. Appl. Math. Stat.* **7**, 714978 (2021).
47. Pecora, L. M. & Carroll, T. L. Master stability functions for synchronized coupled systems. *Phys. Rev. Lett.* **80**, 2109-2112 (1998).
48. Sorrentino, F., Pecora, L. M., Hagerstrom, A. M., Murphy, T. E. & Roy, R. Complete characterization of the stability of cluster synchronization in complex dynamical networks. *Sci. Adv.* **2**, e1501737 (2016).
49. Lodi, M., Sorrentino, F. & Storace, M. One-way dependent clusters and stability of cluster synchronization in directed networks. *Nat. Commun.* **12**, 4073 (2021).
50. Belykh, V. N., Osipov, G. V., Petrov, V. S., Suykens, J. A. K. & Vandewalle, J. Cluster synchronization in oscillatory networks. *Chaos* **18**, 037106 (2008).
51. Della Rossa, F. et al. Symmetries and cluster synchronization in multilayer networks. *Nat. Commun.* **11**, 3179 (2020).

52. Mongillo, G., Barak, O. & Tsodyks, M. Synaptic theory of working memory. *Science* **319**, 1543-1546 (2008).
53. Dörfler, F. & Bullo, F. Synchronization and transient stability in power networks and nonuniform Kuramoto oscillators. SIAM J. Control Optim. 50, 1616-1642 (2012).
54. Simpson-Porco, J. W., Dörfler, F. & Bullo, F. Synchronization and power sharing for droop-controlled inverters in islanded microgrids. Automatica 49, 2603-2611 (2013).
55. Gambuzza, L. V., Buscarino, A., Fortuna, L. & Frasca, M. Memristor-based adaptive coupling for consensus and synchronization. IEEE Trans. Circuits Syst. I Regul. Pap. 62, 1175-1184 (2015).
56. Ignatov, M., Hansen, M., Ziegler, M. & Kohlstedt, H. Synchronization of two memristively coupled van der Pol oscillators. Appl. Phys. Lett. 108, 084105 (2016).
57. Korneev, I. A., Semenov, V. V., Slepnev, A. V. & Vadivasova, T. E. The impact of memristive coupling initial states on travelling waves in an ensemble of the FitzHugh-Nagumo oscillators. Chaos Solitons Fractals 147, 110923 (2021).
58. Kaluza, P. & Cioacă, T. Phase oscillator neural network as artificial central pattern generator for robots. Neurocomputing 97, 115-124 (2012).
59. Dan, H., Yokoi, K., Origane, Y. & Kurabayashi, D. Decentralized particle swarm optimization via coupled oscillators for multi-robot cooperative exploration. Adv. Robot. https://doi.org/10.1080/01691864.2026.2728301 (2026).
60. Holme, P. & Newman, M. E. J. Nonequilibrium phase transition in the coevolution of networks and opinions. Phys. Rev. E 74, 056108 (2006).
61. Kozma, B. & Barrat, A. Consensus formation on adaptive networks. Phys. Rev. E 77, 016102 (2008).

Figure legends

Figure 1 | Adaptive phase-oscillator model and coherence-coupling feedback. a, Oscillators are connected by a fixed sparse network whose existing edge weights w_{ij}

evolve dynamically. **b**, Edges strengthen at rate α when $\cos(\theta_i - \theta_j) > s_c$ and weaken at rate β otherwise. **c**, The ratio $\rho = \alpha/\beta$ distinguishes weakening-dominated, symmetric, and strengthening-dominated adaptation. **d**, Schematic positive feedback in which phase coherence increases the strengthening-edge fraction, raises effective coupling, and promotes further coherence.

Figure 2 | Global synchronization landscape under adaptive coupling. a, Mean Kuramoto order parameter $\langle R \rangle$ across coupling strength K and adaptation-rate ratio ρ in the exploratory scan with fixed $\beta = 0.1$. **b**, Across-realization standard deviation of R. **c**, Representative synchronization curves at selected ρ; marker and line-style differences provide redundant encoding in addition to color. **d**, Three complementary transition estimators: the $R = 0.5$ crossing, maximum local slope, and maximum across-realization SD. The exploratory scan characterizes phenomenology; controlled rate-asymmetry tests at fixed rate budget are shown in Fig. 4.

Figure 3 | Hysteretic synchronization and relaxation-time robustness. a, Forward and backward continuation in K at $\rho = 0.1$; shaded regions show across-realization SD. **b**, Absolute branch separation $|R_{\downarrow} - R_{\uparrow}|$. **c**, Forward and backward branches for $T_{\mathrm{relax}} = 100$, 200, and 400. **d**, Forward and backward $R = 0.5$ crossings versus relaxation time. **e**, Hysteresis width and absolute loop area, each normalized to its value at $T_{\mathrm{relax}} = 100$. Persistence of a large residual loop with increasing relaxation time argues against a purely short-sweep artifact.

Figure 4 | Adaptation-rate asymmetry controls the history-dependent regime. a-c, Low- and high-history branches under a fixed rate budget $\alpha + \beta = 0.2$ for $\rho = 0.1$, 1, and 10. Shading denotes bootstrap 95% confidence intervals across matched realizations. **d**, History-dependent width ΔK obtained from the low- and high-history $R = 0.5$ crossings, with matched-bootstrap 95% confidence intervals. **e**, Relative numerical widths compared with the reduced-theory scaling $\Gamma(\rho)^2$; the vertical axis is logarithmic.

Figure 5 | Cross-initialization reveals non-additive phase-weight memory. a-c, Final synchronization across LL, LH, HL, and HH initializations at $K = 0.8$ for $\rho = 0.1$, 1, and 10. Open symbols show individual realizations and filled symbols show bootstrap means with 95% confidence intervals. **d**, Non-additive phase-weight interaction $I_{\theta W} =$

$R_{HH} - R_{HL} - R_{LH} + R_{LL}$. **e**, Factorial weight-history effect M_W and phase-history effect M_θ, defined as the marginal effect of replacing the corresponding low-history component by its high-history counterpart while averaging over the state of the other component. Error bars denote bootstrap 95% confidence intervals.

Figure 6 | Long-time persistence of history-conditioned synchronization. a,b, Bootstrap mean trajectories and 95% confidence bands for synchronization R and mean edge weight W at $K = 0.8$. **c,d**, Corresponding trajectories at $K = 1.0$. **e**, Late-time paired branch separation $R_{HH} - R_{LL}$ with bootstrap 95% confidence intervals. The high-history branch is stationary to numerical resolution, whereas the low-history branch shows slow residual relaxation while remaining strongly separated.

Supplementary Files

This is a list of supplementary files associated with this preprint. Click to download.

- CommunicationsPhysicsSupplementaryInformation.docx